# Helmholtz Resonator With Sonic Black Hole Neck

**Lihua Peng and Qibo Mao**

*School of Aircraft Engineering, Nanchang HangKong University, 696 South Fenghe Avenue, Nanchang, CN-330063, P. R. China.* E-mail: qbmao@nchu.edu.cn

(Received 30 July 2023; accepted 3 September 2023)

The acoustic performance of a Helmholtz resonator (HR) with a sonic black hole (SBH) neck is investigated in this study both theoretically and experimentally. The proposed SBH neck for a HR consists of a cylindrical tube with a set of rigid thin rings. When the inner radius of the ring is linearly decaying, the SBH effect can be obtained. The sound absorption performance of the proposed HR is then derived based on the transfer matrix method (TMM). Finally, the proposed HRs under different sizes are fabricated by a 3D printing apparatus. The analytical acoustic absorption results are compared to the experimental data obtained from an impedance tube setup. The absorption coefficients from TMM and experiments show a reasonable agreement. When compared to the traditional HR, he main advantage of the proposed HR with a SBH neck is that the broadband sound absorption in a non-HR-resonance frequency range can be achieved.

## 1. INTRODUCTION

The Helmholtz resonator (HR) has been widely used for passive control of narrow-band low frequency noise due to its simple structure.[1–4] It is well-known that the effective sound absorption frequency range of a HR is around its resonance frequency. However, the absorption performance of the HR is deteriorated rapidly in the non-resonance frequency ranges.

To efficiently enlarge the effective sound absorption bandwidth of the HR, a great number of modifications on the HR geometry parameters have been examined. For instances, Tang[5] showed that a HR with a tapped neck can dramatically improve the sound absorption characteristics. Park[6] introduced micro-perforated panels backed by the HRs to enhance sound absorption. Shi and Mak[7] analyzed the HR with a spiral neck, and the results showed that the natural frequency of the HR with a spiral neck can be effectively lowered without changing the cavity volume. Selamet and Lee[8] introduced an extension of the neck into the cavity, the calculated and experimental results showed that the HR natural frequency can be shifted by changing the length, shape, or perforation porosity of the extended neck. Huang et al.[9] further demonstrated that a HR with an extended neck in a cavity can obtain perfect absorption performance. Zhu et al.[10] showed that the HR with a serrated neck can obtain a better sound absorption performance than that of the traditional HR under a high-intensity sound excitation. Selamet et al.[11] investigated the physical parameters of fibrous materials in the HR cavity effect on the resonance frequencies and the transmission loss properties of the HR.

Notice that the sound absorption performance is only applicable to a constant specific frequency as the HR is fabricated. Huang et al.[12] showed that neck-embedded curled HRs can enlarge the tunability of the operating low-frequency sound absorption band. Furthermore, it is found that increasing the thickness of a HR proposed by Huang et al.[12] can effectively enlarge the absorption bandwidth. Bedout et al.[13] have proposed a tunable HR to extend effective absorption bandwidth by adjusting the cavity volume. Currently, various configurations of tunable HRs, including the HR neck length adjusting or opening adjusting, have been reported.[14–16] Recently, a HR with sweeping natural frequency was proposed by using a time-varying Proportional-Integral (PI) controller.[17] The noise can be blindly controlled in the sweeping frequency range of the sweeping HR.

The intention of enlarging the resonance frequency bandwidth of a HR, (two degrees of freedom (two-DOF) HR) by using a pair of neck and cavity connected in series has also been widely investigated. For examples, Doria[18] presented an analytical two-DOF HR model, the results showed that the natural frequencies of a two-DOF HR depend on the individual natural frequency of each HR and volume ratio. Xu et al.[19] presented the closed-form expression for the transmission loss of the two-DOF HR. Tang et al.[20] presented the experimental sound absorption performance for a two-DOF HR based on the impedance tube method. The two-DOF HR can also be designed by replacing the rigid wall of the cavity with a flexible end panel.[21,22] Following consideration of the application under the multiple natural frequencies, the HR array with different natural frequencies has also been frequently used as a basic concept in the design of broadband acoustic metamaterials and acoustic metasurfaces.[23–26]

Generally speaking, the effective sound absorption bandwidth of HR-based acoustic absorbers depends on their natural frequencies. How to design a modified HR with effective sound absorption performance in other frequency ranges remains an important question to be answered.

Recently, Acoustic black hole (ABH) has been investigated intensively due to its excellent ability on broadband structural vibration control and sound insulation. Notice that there are two types of ABH structures considered in previous publications.[27–31] The wedge-shaped structures, where bending waves propagate with decreasing velocity as their amplitude increases, have been termed as ABH.[27,28] A tube with graded retarding rings for sound absorption is normally termed as sonic black hole (SBH).[30,31] The recent review papers give an exhaustive literature survey on ABH structures for vibration control.[27,28] Zhou and Yu[29] introduced ABHs panel in a HR cavity to broaden the bandwidth of the natural frequency. On the other hand, Air-borne SBH proposed by Mironov and Pislyakov[30] has a wide effective sound absorption frequency range in air due to the slow-sound effect. SBH absorber studied by Mironov and Pislyakov[30] contains a cylindrical duct comprised of a series of rigid rings with gradually decreasing inner radius. The sound speed through SBH will gradually decrease through the structure leading to the SBH effect. Ideally, the incident waves do not reflect back because the sound speed will tend to be zero at the end of the SBH. Mironov and Pislyakov[31] presented the experimental sound absorption performances for various modifications of SBH structures.

In recent times, the transfer matrix method (TMM) has been imposed to study the reflection coefficient for linear and quadratic SBH.[32,33] The SBH physical parameters (such as ring thickness, the number of rings, the minimum radius of the rings, and damping loss factors) effect on absorption performance was discussed. Hollkamp and Semperlotti[34] imposed a fractional order model to analyze the absorbing performance of a duct with SBH termination. Zhang and Cheng,[35] Li et al.,[36] and Liang et al.[37] introduced micro-perforated panels in a SBH cavity to create hybrid acoustic absorber and achieve broadband and low-frequency sound absorption. In addition, the viscous and thermal losses as well as the role of resonances of the side-cavities in SBHs influence on absorption performance has been analyzed in detail.[38–40]

Mi et al.[41] introduced an open-end quadratic SBH without rigid termination. The calculated and experimental results showed that sound reflection and transmission of the open-ended SBH can be simultaneously reduced. In a recent work, by Mi et al.[42] the sound transmission loss for a periodic open-ended SBH both analytically and experimentally were studied further.

Considering the sound absorption properties of the HR and SBH, it is possible to establish a coupled acoustic absorber by combining the HR and SBH. In this study, an open-end SBH is used as a HR neck to achieve effective broadband sound absorption in non-HR-resonance frequency ranges. The goal of the present study is twofold. First, it is the goal to investigate theoretically and experimentally the acoustic performance of a HR with an SBH neck. Second, it is also the goal to examine the influence of geometrical parameters of the proposed HR on sound absorption performance.

The study starts with describing the geometric design of a HR with an SBH neck; then, an analytical prediction method is established to evaluate the sound absorption performance of the proposed HR based on the TMM. Third, the numerical and experimental results are given, and their performance is compared to validate the effectiveness of the model. Fourth, the influence of HR geometrical parameters on sound absorption are studied. These include the length of an SBH neck, inner radius of the end ring in an SBH neck, the damping factor and the length of an additional neck. Finally, some useful conclusions are drawn and illustrated.

## 2. GEOMETRIC DESIGN OF HR WITH SBH NECK

A schematic diagram for the proposed HR with an SBH neck model is shown in Fig. 1(a). Unlike the traditional HR, the SBH neck considered in this study is a cylindrical tube with an array of $N$ regularly-spaced rigid-walled thin rings. The inner radii of the rings are linearly decreasing. In the analysis of the proposed HR, for simplicity, the HR is assumed to have rigid walls and the cross section of the HR is circular. The thickness of the ring is sufficiently thin and thus can be reasonably neglected. The cross-sectional view of the proposed HR model is presented in Fig. 1(b). $R_{sbh}$ and $L_{sbh}$ are the radius and length of the SBH neck, respectively; $r_n$ is the inner radius of the $n$th ring; $d_n$ is the distance between the $(n-1)$th and $n$th ring. An additional neck with length $L_{neck}$ is used to connect the SBH neck and the backing cavity. The radius of the additional neck is $R_{neck}$, which is equal to that of the SBH end ring. $L_{HR}$ and $R_{HR}$ are the length and radius of HR cavity, respectively. Axes of symmetry of the SBH neck, additional neck and the cavity are assumed to coincide. From Fig. 1(b), the inner radius of $n$th ring can be written as:

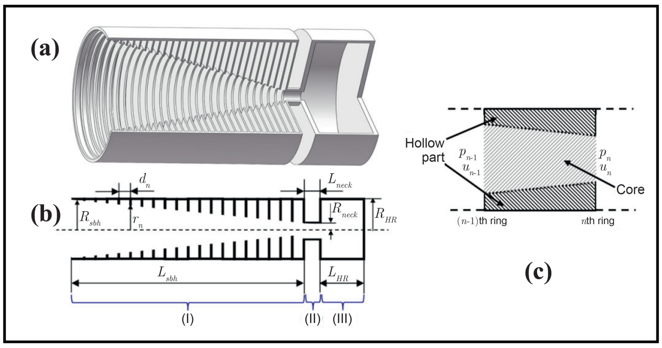


**Figure 1.** (a) Geometry illustration for HR with SBH neck; (b) Cross-sectional view of HR with SBH neck; (c) Detailed schematic of $n$th element of the SBH neck.

$$r_n = \frac{R_{sbh} - r_N}{L_{sbh}} \left( L_{sbh} - \sum_{i}^{n} d_i \right) + r_N, n = 0, 1, 2, \ldots, N. \tag{1}$$

## 3. THEORETICAL MODEL FOR THE HR WITH SBH NECK

Assume that the characteristic dimension of the HR is much smaller than the acoustic wavelength for the frequencies of interest. This allows the plane wave propagation in a HR. The TMM can be used to evaluate the acoustic impedance of the proposed HR shown in Fig. 1. Then the sound absorption coefficient can be determined based on the acoustic pressure and particle velocity at the HR mouth.

The proposed HR can be divided into three regions, i.e., the SBH neck (I), the additional neck (II) and the backing cavity (III), as presented in Fig. 1(b). The SBH neck is further divided into $N$ longitudinal cylindrical duct elements. Each element can also be divided into two parts, such as the core of the duct between the two neighbouring rings and the hollow part between two rings, as shown Fig. 1(c). According to the papers of Guasch et al.,[32,33] the transfer matrix for the $n$th cylindrical element can be expressed as Eq. (2). Where $p_{n-1}$, $u_{n-1}$ and $p_n$, $u_n$ and are the acoustic pressures and acoustic particle velocities at the $(n-1)$th and $n$th ring, respectively; $Y_n$ is the cavity admittance due to the hollow part shown in Fig. 1(c); $S_n = \pi r_n^2$ is the cross-sectional open area of the $n$th ring; $d_n$ is the distance between $(n-1)$th and $n$th ring; $j$ is the imaginary unit. $Z_{eff,n}$ and $k_{eff,\,n}$ are respectively the effective impedance and the effective wavenumber of the $n$th

$$\begin{bmatrix} p_{n-1} \\ u_{n-1} \end{bmatrix} = \begin{bmatrix} cos\left(k_{eff,n}d_n\right) & jsin\left(k_{eff,n}d_n\right) Z_{eff,n}/S_n \\ jsin\left(k_{eff,n}d_n\right) S_n/Z_{eff,n} & cos\left(k_{eff,n}d_n\right) \end{bmatrix} \begin{bmatrix} 1 & 0 \\ Y_n & 1 \end{bmatrix} \begin{bmatrix} p_n \\ u_n \end{bmatrix}, n = 1, 2, \ldots, N. \quad (2)$$

cylindrical element, with the expression of:[43]

$$Z_{eff,n} = \rho_{eff,n} c_{eff,n} \text{ and } k_{eff,n} = \frac{\omega}{c_{eff,n}}; \quad (3)$$

where $\omega$ is the angular frequency, $\rho_{eff,n}$ and $c_{eff,n}$ are respectively the frequency-dependent complex density and sound speed of air in the $n$th cylindrical element. Based on the equivalent fluid model,[43] $\rho_{eff,n}$ and $c_{eff,n}$ can be expressed as,

$$\rho_{eff,n} = \frac{\rho_0}{F_{a,n}} \text{ and } c_{eff,n} = c_0 \sqrt{\frac{F_{a,n}}{\gamma - (\gamma - 1) F_{b,n}}}; \quad (4)$$

with $F_{a,n} = 1 - \frac{2J_1\left(r_n\sqrt{-j\omega\rho_0/\mu_0}\right)}{r_n\sqrt{-j\omega\rho_0/\mu_0}J_0\left(r_n\sqrt{-j\omega\rho_0/\mu_0}\right)}$; $F_{b,n} = 1 - \frac{2J_1\left(r_n\sqrt{-j\omega\gamma\rho_0 C_{\nu 0}/\kappa_0}\right)}{r_n\sqrt{-j\omega\gamma\rho_0 C_{\nu 0}/\kappa_0}J_0\left(r_n\sqrt{-j\omega\gamma\rho_0 C_{\nu 0}/\kappa_0}\right)}$; where $\rho_0 = 1.21$ kg/m$^3$ is the air density; $c_0 = 340$ m/s is the lossless speed of sound; $\gamma = 1.4$ is the ratio of specific heat; $\mu_0 = 1.8 \times 10^{-5}$ Pa is the dynamic viscosity; $C_{\nu 0} = 718$ J(kg.K) and $\kappa_0 = 0.0258$ W/(m.K) are the heat capacity at constant volume and the thermal conductivity, respectively. $J_1$ and $J_0$ are the zero and the first order Bessel functions of the first kind.

The cavity admittance $Y_n$ can be approximated by:[32,41]

$$Y_n = j\frac{\omega}{\rho_{eff,n}^{cav}\left(c_{eff,n}^{cav}\right)^2} V_n^{cav}; \quad (5)$$

where $V_n^{cav}$ is the volume of the $n$th hollow part, which can be considered as the difference of a cylinder and a truncated cone, such as,

$$V_n^{cav} = \pi d_n \left[R^2 - \frac{1}{3}\left(r_n^2 + r_{n+1}^2 + r_n r_{n+1}\right)\right]. \quad (6)$$

Based on study of Stinson,[43] the plane-wave propagation in the $n$th hollow part by Stinson[43] is employed in this study. The effective air density $\rho_{eff,n}^{cav}$ and sound speed $c_{eff,n}^{cav}$ in Eq. (5) for the $n$th hollow part can be expressed as,

$$\rho_{eff,n}^{cav} = \frac{\rho_0}{F_\alpha}; \quad (7)$$

$$c_{eff,n}^{cav} = c_0 \sqrt{\frac{F_\alpha}{\gamma - (\gamma - 1) F_\beta}}; \quad (8)$$

where $F_\alpha = 1 - \frac{tanh\left((d_n/2)\sqrt{j\omega\rho_0/\mu_0}\right)}{(d_n/2)\sqrt{j\omega\rho_0/\mu_0}}$, $F_\beta = 1 - \frac{tanh\left((d_n/2)\sqrt{j\omega\gamma\rho_0 C_{\nu 0}/\kappa_0}\right)}{(d_n/2)\sqrt{j\omega\gamma\rho_0 C_{\nu 0}/\kappa_0}}$.

From Eq. (2), the overall transfer matrix of the SBH neck (region I) can be obtained by connecting each SBH element through Eq. (9).

Similarly, the transfer matrices for regions II and III shown in Fig. 1(b) can be expressed by Eqs. (10), (11), (12). Where $p_N$, $u_N$ and $p_{neck}$, $u_{neck}$ are the acoustic pressures and particle velocities at the input and output end of the additional neck, respectively. $p_C$, $u_C$ are the acoustic pressures and particle velocity at the end wall of the HR cavity. $Z_h$ and $k_h$ ($h$ = *neck* or *HR*) are the effective wavenumber and the effective impedance for the neck and cavity, respectively. $Z_h$ and $k_h$ can be obtained by using Eq. (4).

By connecting $\boldsymbol{T}_{SBH}^{I}$, $\boldsymbol{T}_{neck}^{II}$ and $\boldsymbol{T}_{cavity}^{III}$ and based on the TMM approach, the inlet acoustic pressure $p_0$ and particle velocity $u_0$ for proposed HR can be obtained as:

$$\begin{bmatrix} p_0 \\ u_0 \end{bmatrix} = \boldsymbol{T}_{SBH}^{I}\boldsymbol{T}_{neck}^{II}\boldsymbol{T}_{cavity}^{III} \begin{bmatrix} p_C \\ u_C \end{bmatrix} = \boldsymbol{T}_{total} \begin{bmatrix} p_C \\ u_C \end{bmatrix}; \quad (13)$$

where $\boldsymbol{T}_{total} = \boldsymbol{T}_{SBH}^{I}\boldsymbol{T}_{neck}^{II}\boldsymbol{T}_{cavity}^{III}$ is the overall transfer matrix for the HR.

Considering the end wall of the backing cavity of the HR is rigid, it means that the particle velocity $u_C$ is equals to zero. From Eq. (13), the effective acoustic impedance of the HR can be expressed as,

$$Z_{in} = \frac{p_0}{u_0} = \frac{T_{total}(1,1)}{T_{total}(2,1)}; \quad (14)$$

where $T_{total}(1,1)$ and $T_{total}(2,1)$ are the elements of $\boldsymbol{T}_{total}$.

Once the effective acoustic impedance $Z_{in}$ in Eq. (14) is determined, the normal sound absorption coefficients of the HR can be expressed as,

$$\alpha = 1 - \left|\frac{Z_{in} - Z_0/S_0}{Z_{in} + Z_0/S_0}\right|^2. \quad (15)$$

# 4. ACOUSTIC CHARACTERISTICS OF HR WITH SBH NECK

## 4.1. Absorbing Performance Validation (Model Validation)

### 4.1.1. Experimental Setup

For the experiment, four HR samples were made of photosensitive resin material by using 3D printing technology. The HR samples were arranged in a cylindrical case with an outer diameter of 99 mm to fit in the impedance tube, as shown in Fig. 2. The SBH necks in all samples have 30 rings. The thickness of each ring is 0.7 mm. The distance between adjacent rings is 2.3 mm. The inner radii of the SBH neck and cavity are 47.5 mm. Other geometric parameters for each sample are listed in Table I. Based on the two-microphone transfer function method according to the ISO standard 10534-2,[44] the sound absorption coefficient was measured in an impedance tube (AWA8551T, Aihua Inc., China) with inner diameter of 100 mm. The experimental setup photo is shown in Fig. 3. The distance between the loudspeaker, two microphones and the sample are also presented in Fig 3. The valid frequency range is 60–1600 Hz based on this setup arrangement. Two free-field microphones (AWA14435, Aihua Inc., China) with built-in pre-amplifier (AWA14614E, Aihua Inc., China) were used. A dynamic signal analyzer (AWA6290B, Aihua Inc., China) was used to acquire the measured output signals of two microphones. Finally, a post-processing software (AWA6290B,

$$\begin{bmatrix} p_0 \\ u_0 \end{bmatrix} = \prod_{n=1}^{N} \boldsymbol{T}_n^I \begin{bmatrix} p_N \\ u_N \end{bmatrix} = \boldsymbol{T}_{SBH}^I \begin{bmatrix} p_N \\ u_N \end{bmatrix}; \tag{9}$$

where $\boldsymbol{T}_n^I = \begin{bmatrix} cos\left(k_{eff,n}d_n\right) & jsin\left(k_{eff,n}d_n\right) Z_{eff,n}/S_n \\ jsin\left(k_{eff,n}d_n\right) S_n/Z_{eff,n} & cos\left(k_{eff,n}d_n\right) \end{bmatrix} \begin{bmatrix} 1 & 0 \\ Y_n & 1 \end{bmatrix}$, $\boldsymbol{T}_{SBH}^I = \prod_{n=1}^{N}, \boldsymbol{T}_n^I$ is the transfer matrix for SBH neck.

$$\boldsymbol{T}_{neck}^{II} = \begin{bmatrix} cos\left(k_{neck}L_{neck}\right) & jsin\left(k_{neck}L_{neck}\right) Z_{neck}/S_{neck} \\ jsin\left(k_{neck}L_{neck}\right) S_{neck}/Z_{neck} & cos\left(k_{neck}L_{neck}\right) \end{bmatrix}; \tag{10}$$

$$\boldsymbol{T}_{cavity}^{III} = \begin{bmatrix} cos\left(k_{HR}L_{HR}\right) & jsin\left(k_{HR}L_{HR}\right) Z_{HR}/S_{HR} \\ jsin\left(k_{HR}L_{HR}\right) S_{HR}/Z_{HR} & cos\left(k_{HR}L_{HR}\right) \end{bmatrix}; \tag{11}$$

$$\begin{bmatrix} p_N \\ u_N \end{bmatrix} = \boldsymbol{T}_{neck}^{II} \begin{bmatrix} p_{neck} \\ u_{neck} \end{bmatrix}, \begin{bmatrix} p_{neck} \\ u_{neck} \end{bmatrix} = \boldsymbol{T}_{cavity}^{III} \begin{bmatrix} p_C \\ u_C \end{bmatrix}. \tag{12}$$

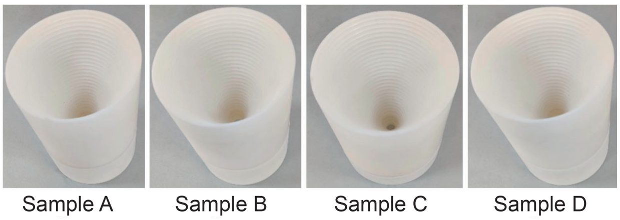


**Figure 2.** Photographs of fabricated samples.

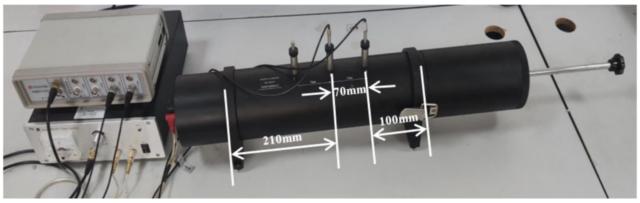


**Figure 3.** The experimental setup photo for measurement of sound absorption coefficient by using impedance tube.

**Table 1.** Physical parameters of the HRs. (unit: mm).

| | Sample A | Sample B | Sample C | Sample D |
|---|---|---|---|---|
| $L_{neck}$ | 13 | 6 | 6 | 7 |
| $R_{neck}$ | 3 | 4.5 | 4.5 | 3 |
| $L_{HR}$ | 48 | 48 | 25 | 48 |

Aihua Inc., China) was used to obtain the experimental sound absorption coefficients.

### 4.1.2. Experimental Results and Validation

To demonstrate the validity of the proposed HR analytical model in Section 3, the calculated sound absorption coefficient is first compared with that obtained from experiment.

The predicted and measured sound absorption coefficients of the HRs are presented in Fig. 4. For comparison, the results for traditional HR (removing SBH neck) are also presented in Fig. 4.

In Fig. 4, it is seen that the trend of the absorption coefficient between the predicted and the measured results have a good agreement at the low frequency region (below 600 Hz). Compared to the traditional HR, the HR with an SBH neck has lower first resonance frequency. However, it should be noted that the thickness of the traditional HR is 90 mm shorter than the HR with an SBH neck. If the SBH necks are replaced by traditional HR necks, the first resonance frequencies for samples A, B, C and D would be tuned from 106 Hz, 167 Hz, 237 Hz and 128 Hz to 47 Hz, 71 Hz, 99 Hz and 49 Hz, respectively. It means that the SBH neck cannot lower the first resonance frequency effectively. The levels of measured absorption coefficients for all samples are generally higher than predicted results above 600 Hz. The possible reason for these deviations between experimental and predictions may result from the imperfect manufacture of the test samples and the inevitable gap between the sample and the impedance tube. Nevertheless, the calculated and the measured absorption coefficients have a good agreement and general trend. The proposed HR with an SBH neck can obtain effective acoustic absorption in wideband non-HR-resonance frequency range. For example, additional half-absorption bandwidth (absorption coefficient $\alpha > 0.5$) for HR with an SBH neck from 582 Hz to 1.60 kHz in Fig. 4(a), from 635 Hz to 1.60 kHz in Fig. 4(b), from 666 Hz to 1.60 kHz in Fig. 4(c) and from 658 Hz to 1.6 kHz in Fig. 4(d), can be obtained based on the measured results. The acoustic performance for a HR with an SBH neck is drastically different from a traditional HR, because the traditional HR only has a narrow effective absorption frequency band. The sound absorption coefficients for traditional HRs in the non-resonance frequency ranges have almost no sound absorption effect.

Furthermore, broadband quasi-perfect absorption (the absorption coefficient $\alpha > 0.9$) can also be found in Fig. 4. For example, broadband quasi-perfect absorption in [900, 1320] Hz and [1514, 1600] Hz are experimentally observed for sample A (Fig. 4(a)). As presented in Fig. 4(b), sample B experimentally exhibits quasi-perfect absorption in [700 920] Hz, [1110 1360] Hz and [1524 1600] Hz. Similar experimental results can also be found for samples C and D.

To further investigate the absorption mechanism of the proposed HR, the reflection coefficients $R = (Z_{in} - Z_0/S_0)/(Z_{in} + Z_0/S_0)$ in the complex frequency plane[45,46] is analyzed by using the complex frequency $f_c = f_r + jf_i$. The additional damping in the system can be introduced by the imaginary part $f_i$. The color maps of calculated $20\log_{10}(|R|)$ for four samples listed in Table 1 in the complex frequency plane are presented in Fig. 5. Three pairs of zeros and poles can be found in the complex frequency plane. Clearly, the real frequency values of these pairs of zeros and poles are corresponding to the frequencies of the absorption peaks in Fig. 4. The first zero/pole pair is due to the HR without the SBH neck, while the second and third zero/pole pairs are due to the SBH effect. If distance from the real axis to the pole is larger, a wider half-absorption bandwidth can

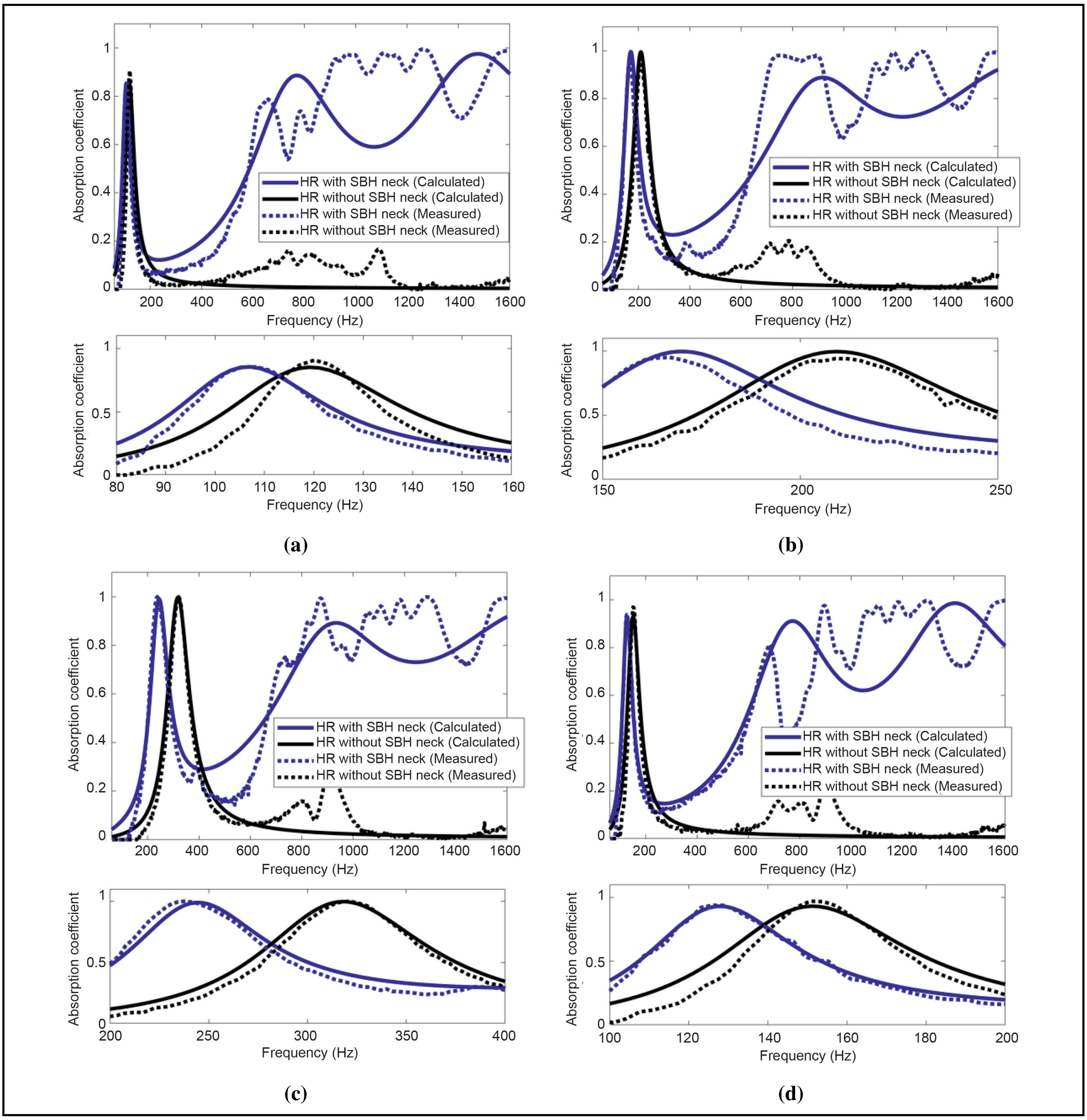


**Figure 4.** The predicted and measured sound absorption coefficients of the HR with and without an SBH neck for (a) sample A; (b) sample B; (c) sample C and (d) sample D.

be observed in Fig. 4. According to complex frequency plane method,[45,46] the perfect absorption can be realized when the zero barely crosses the real axis. From Fig. 5, the perfect absorption condition is basically satisfied by the first and third zeros of all samples. All samples are under-damped around the frequency of the second zero, because it is located above the real axis. It is understandable because no additional damping material is added in the proposed HRs.

To experimentally investigate the damping materials influence in the sound absorption performance, Figure 6 shows the calculated and experimental sound absorption coefficients when the inner wall of the SBH neck for the sample A is covered with sponges of 2 mm thickness. It is found that the sound absorption performance above 600 Hz can be improved significantly when the porous material is adding to the proposed HR. Good agreements can be observed between the prediction and measured results when the complex sound speed in Eq. (4) is chosen as $c_{eff,n} = c_0(1 + 0.265j)$ in a calculation based on TMM. However, compared Fig. 6 to Fig. 4(a), it can be found that the absorption peak at first resonance is reduced from 0.85 to 0.58 according to measured results. It means that low frequency sound absorption performance could be reduced due to the sponges in the SBH neck. Optimizing the porous material location in the SBH neck may achieve a better sound absorption effect, which needs to be further explored in future studies.

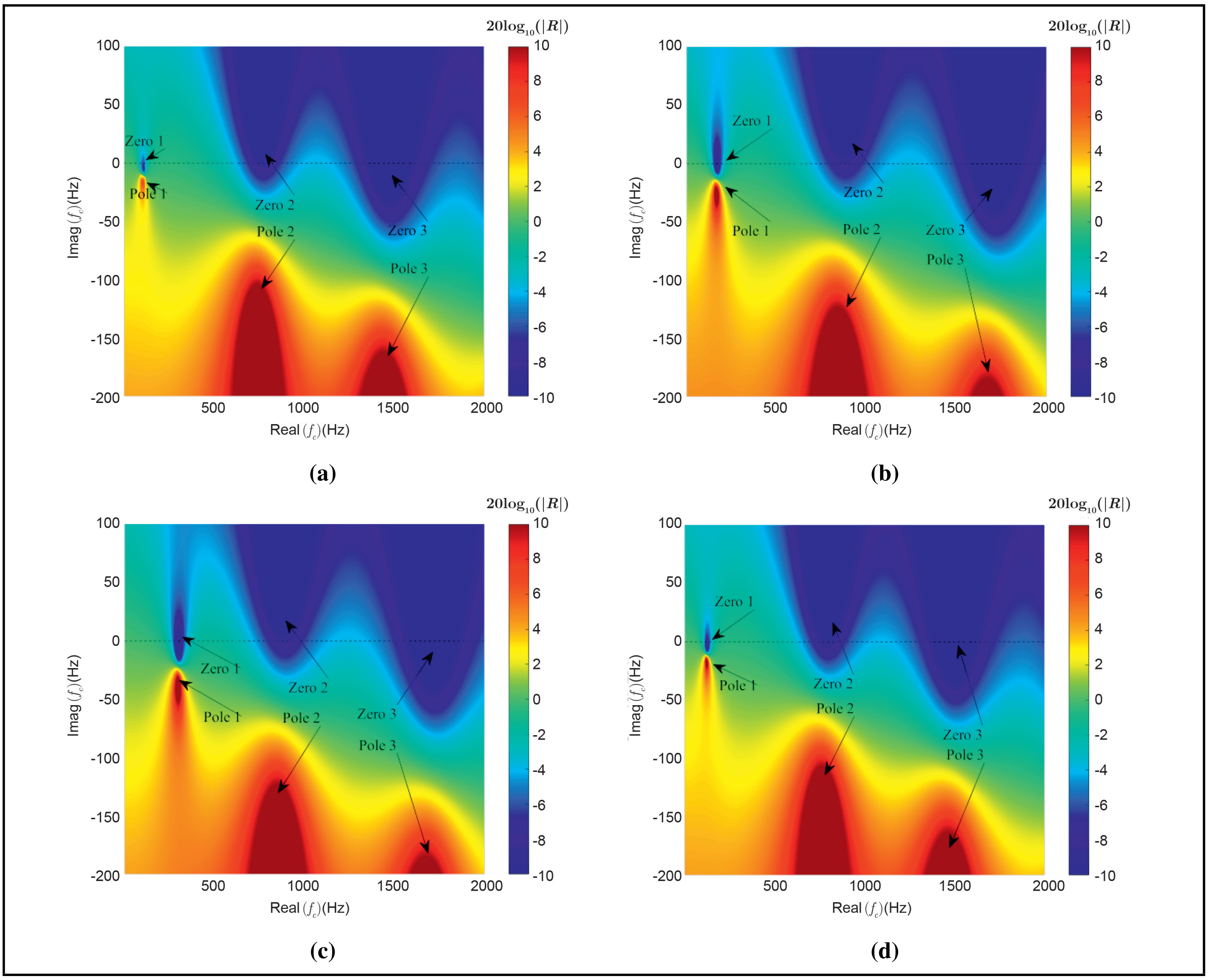


**Figure 5.** Contour of 20$\log_{10}(|R|)$ in the complex frequency plane for (a) sample A; (b) sample B; (c) sample C and (d) sample D.

## 4.2. Acoustic Performance Influence Geometric Parameters of a HR with the SBH Neck

To further investigate the sound absorption performance of the proposed HR, the geometric parameters of the HR effect on absorption coefficient calculated from the proposed theoretical model will be discussed in this subsection.

In Figs. 4, 5, 6 it is found that the four main geometric variables, such as length of SBH neck $L_{sbh}$, radius of additional neck $R_{neck}$ (equal to inner radius of the end ring $r_N$ of the SBH neck, as shown in Fig. 1), damping factor $\zeta$ and length of additional neck $L_{neck}$, have significant effects on the absorption performance of proposed HR. For simplicity, assume that the radius of the SBH neck and a HR cavity, the ring number in the SBH and the cavity length are the same as sample A (such as $R_{sbh} = R_{HR} = 47.5$ mm, $N = 30$ and $L_{HR} = 48$ mm) and are used for the following calculations. Figure 7 shows the calculated absorption contours under different geometric variables. It was found that more absorption bands appear as the length of the SBH neck $L_{sbh}$ increases for a given frequency range (0–2000 Hz in this case). The absorption bands shift to lower frequencies when $L_{sbh}$ increases. The shifting trend gets less obvious for the first absorption band, as shown in Fig. 7(a). By contrast, the absorption peaks shift to higher frequencies if the radius of an additional neck $R_{neck}$ is increased. Furthermore, the peak values of the first two absorption bands will also be deteriorated along when the SBH radius rises, as presented in Fig. 7(b). It means that the relative long $L_{sbh}$ and small $R_{neck}$ are beneficial for low frequency absorption.

The effects of damping on sound absorption performance have been presented in Fig. 7(c) by replacing $c_{eff,n}$ in Eq. (4) and $c^{cav}_{eff,n}$ in Eq. (7) as different complex sound speed, such as $c_{eff,n} = c^{cav}_{eff,n} = c_0(1+\zeta)$, $\zeta$ is the damping parameter with positive constant. It was found that sound absorption performance is influenced significantly by damping factor $\zeta$. From Fig. 7(c), it can be found that adding damping can improve the acoustic performance of the proposed HR. However, the peak value of the first absorption band deteriorates rapidly. This phenomenon can also been observed in the experimental results (see Fig. 6).

If the length of additional neck $L_{neck}$ is increased, all absorption bands shift to low frequencies, as shown in Fig. 7(d). The shifting trend gets more obvious for $L_{neck}$ varied from 0 to 4 mm. As compared in Fig. 7(d) to Fig. 7(a), it was found that increasing the length of the additional neck is a more effective

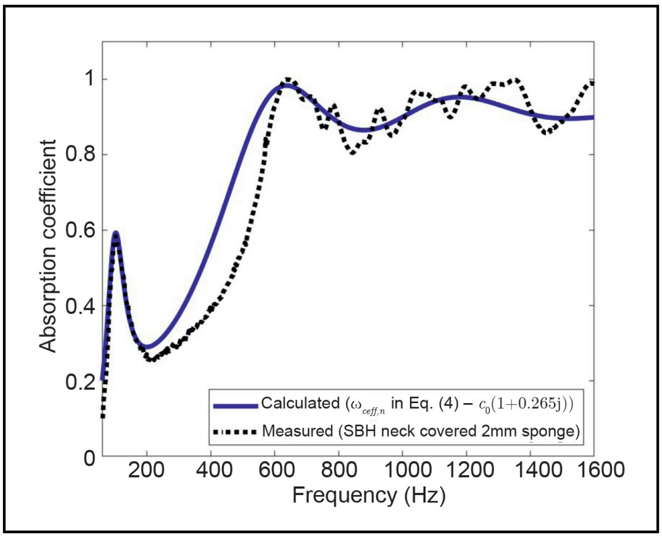


**Figure 6.** The predicted and measured sound absorption coefficients for sample A when the SBH neck is covered by a 2 mm sponge.

way to decrease the first resonant frequency, while increasing the length of the SBH neck can shift other absorption bands to lower frequencies significantly.

## 5. CONCLUSIONS

In this study, acoustic characteristics of a HR with an open-end SBH neck have been analyzed theoretically and experimentally. A simple theoretical model based on TMM is established to evaluate the sound absorption performance of a HR with an SBH neck. Compared to the traditional HR, the HR with an SBH neck can obtain effective acoustic absorption in a wideband non-HR-resonance frequency range. The calculated and experimental results are presented to verify the effectiveness of the TMM model. The influence of geometric parameters on sound absorption is also studied. It is worth mentioning that the traditional HR can be easily modified by adding an additional SBH neck, this has a potential application for simultaneous control of tonal noise at a targeted low frequency ($<$ 400 Hz) and broadband noise at moderate and high frequency ranges.

## CONFLICT OF INTEREST

The authors declare that they have no known competing financial interests or personal relationships that could have appeared to influence the work reported in this paper.

## ACKNOWLEDGEMENTS

This work was sponsored by the National Natural Science Foundation of China (no. 12364058 and no. 51975266) and the Aeronautical Science Foundation of China (no. 2020Z073056001).

## REFERENCES

[1] Esteve, S. J. and Johnson, M. E. Reduction of sound transmission into a circular cylindrical shell using distributed vibration absorbers and Helmholtz resonators, *J. Acoust. Soc. Am.*, **112**, 2840–2848, (2002). https://doi.org/10.1121/1.1514933

[2] Corà, R., Martins, C .A., and Lacava, P. T. Acoustic instabilities control using Helmholtz resonators, *Appl. Acoust.*, **77**, 1–10, (2014). https://doi.org/10.1016/j.apacoust.2013.09.013

[3] Pietrzko, S. and Mao, Q. New results in active and passive control of sound transmission through double wall structures, *Aerosp. Sci. Technol.*, **12**(1), 42–53, (2008). https://doi.org/10.1016/j.ast.2007.10.006

[4] Mao, Q. and Pietrzko, S. Experimental study for control of sound transmission through double glazed window using optimally tuned Helmholtz resonators, *Appl. Acoust.*, **71**, 32–38, (2010). https://doi.org/10.1016/j.apacoust.2009.07.007

[5] Tang, S. K. On Helmholtz resonators with tapered necks, *J. Sound Vib.*, **279**, 1085–1096, (2005). https://doi.org/10.1016/j.jsv.2003.11.032

[6] Park, S. H. Acoustic properties of micro-perforated panel absorbers backed by Helmholtz resonators for the improvement of low-frequency sound absorption, *J. Sound Vib.*, **332**, 4895–4911, (2013). https://doi.org/10.1016/j.jsv.2013.04.029

[7] Shi, X. and Mak, C. M. Helmholtz resonator with a spiral neck, *Appl. Acoust.*, **99**, 68–71, (2015). https://doi.org/10.1016/j.apacoust.2015.05.012

[8] Selamet, A. and Lee, I. Helmholtz resonator with extended neck, *J. Acoust. Soc. Am.*, **113**(4), 1975–1985, (2003). https://doi.org/10.1121/1.1558379

[9] Huang, S., Fang, X., Wang, X., Assouar, B., Cheng, Q., and Li, Y. Acoustic perfect absorbers via Helmholtz resonators with embedded apertures, *J. Acoust. Soc. Am.*, **145**(1), 254–262, (2019). https://doi.org/10.1121/1.5087128

[10] Zhu, J., Qu, Y., Gao, H., and Meng, G. Nonlinear sound absorption of Helmholtz resonators with serrated necks under high-amplitude sound wave excitation, *J. Sound Vib.*, **537**, 117197, (2022). https://doi.org/10.1016/j.jsv.2022.117197

[11] Selamet, A., Xu, M. B., Lee, I.J., and Huff, N. T. Helmholtz resonator lined with absorbing material, *J. Acoust. Soc. Am.*, **117**, 725–733, (2005). https://doi.org/10.1121/1.1841571

[12] Huang, S., Fang, X., Wang, X., Assouar, B., Cheng, Q., and Li, Y. Acoustic perfect absorbers via spiral metasurfaces with embedded apertures, *Appl. Phys. Lett.*, **113**, 233501, (2018). https://doi.org/10.1063/1.5063289

[13] Bedout, J. M., Franchek, M. A., Bernard, R. J., and Mongeau, L. Adaptive-passive noise control with self-tuning resonators, *J. Sound Vib.*, **202**, 109–123, (1997). https://doi.org/10.1006/jsvi.1996.0796

[14] Nagaya, K., Hano, Y., and Suda, A. Silencer consisting of two-stage Helmholtz resonator with auto-tuning control, *J. Acoust. Soc. Am.*, **110**, 289–295, (2001). https://doi.org/10.1121/1.1370524

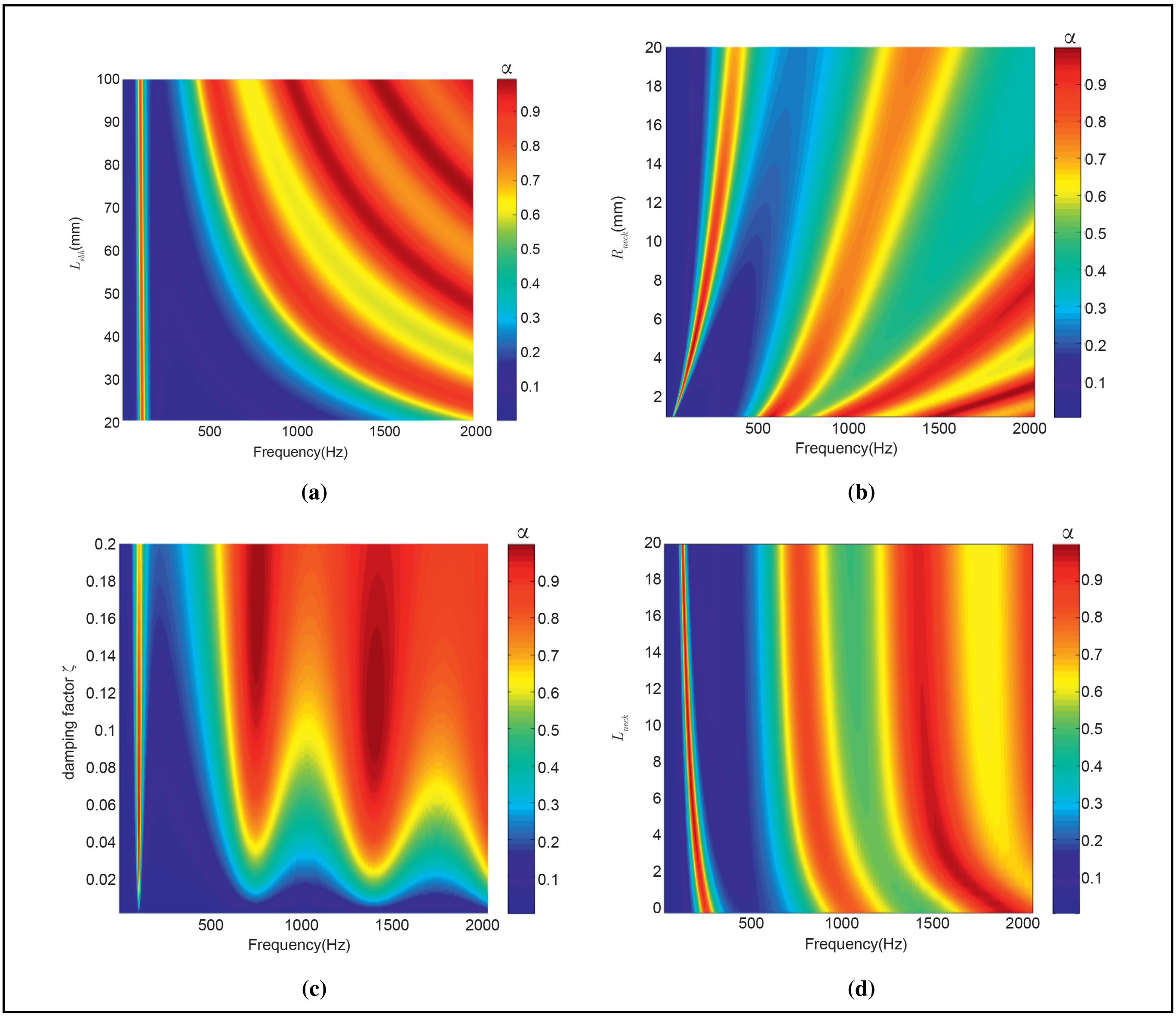


**Figure 7.** The calculated sound absorption coefficients of sample A under different (a) lengths of SBH neck $L_{sbh}$; (b) radii of additional neck $R_{neck}$; (c) damping factors $\zeta$ and (d) lengths of additional neck $L_{neck}$.


[15] Yun, Y. and Mak, C. M. The theoretical fundamentals of an adaptive active control using periodic Helmholtz resonators for duct-borne transmission noise in ventilation systems, *Building Serv. Eng. Res. Technol.*, **34**(2), 195–201, (2010). https://doi.org/10.1177/0143624410389578

[16] Esteve, S. J. and Johnson, M. E. Adaptive Helmholtz resonators and passive vibration absorbers for cylinder interior noise control, *J. Sound Vib.*, **288**, 1105–1130, (2005).

[17] Mao, Q., Li, S., and Liu, W. Development of a sweeping Helmholtz resonator for noise control, *Appl. Acoust.*, **141**, 348–354, (2018). https://doi.org/10.1016/j.jsv.2005.01.017

[18] Doria, A. Control of acoustic vibrations of an enclosure by means of multiple resonators, *J. Sound Vib.*, **181**, 673–685, (1995). https://doi.org/10.1006/jsvi.1995.0165

[19] Xu, M. B., Selamet, A., and Kim, H. Dual Helmholtz resonator, *Appl. Acoust.*, **71**, 822–829, (2010). https://doi.org/10.1016/j.apacoust.2010.04.007

[20] Tang, S. K., Ng, C. H., and Lam, E. Y. L. Experimental investigation of the sound absorption performance of compartmented Helmholtz resonators, *Appl. Acoust.*, **73**(9), 969–976, (2012). https://doi.org/10.1016/j.apacoust.2012.03.016

[21] Sanada, A. and Tanaka, N. Extension of the frequency range of resonant sound absorbers using two-degree-of-freedom Helmholtz-based resonators with a flexible panel, *Appl. Acoust.*, **74**, 509–516, (2013). https://doi.org/10.1016/j.apacoust.2012.09.012

[22] Nudehi, S. S., Duncan, G. S., and Farooq, U. Modeling and experimental investigation of a Helmholtz resonator with a flexible plate, *J. Vib. Acoust.*, **135**, 041102, (2013). https://doi.org/10.1115/1.4023810

[23] Jena, D. P., Dandsena, J., and Jayakumari, V. G. Demonstration of effective acoustic properties of different configurations of Helmholtz resonators, *Appl. Acoust.*, **155**, 371–382, (2019). https://doi.org/10.1016/j.apacoust.2019.06.004

[24] Ryoo, H. and Jeon, W. Broadband sound absorption using multiple hybrid resonances of acoustic metasurfaces, *Int. J. Mech. Sci.*, **229**, 107508, (2022). https://doi.org/10.1016/j.ijmecsci.2022.107508

[25] Yang, C., Zhong, T., Li, J., You, S., Yang, S., Zhang, H., and Zheng, Z. Extended tube acoustic metamaterial: Its modeling and application to a kitchen hood, *Appl. Acoust.*, **185**, 108398, (2022). https://doi.org/10.1016/j.apacoust.2021.108398

[26] Rajendran, V., Piacsek, A., and Echenagucia, T. M. Design of broadband Helmholtz resonator arrays using the radiation impedance method, *J. Acoust. Soc. Am.*, **151**(1), 457–466, (2022). https://doi.org/10.1121/10.0009317

[27] Pelat, A., Gautier, F., Conlon, S. C., and Semperlotti, F. The acoustic black hole: a review of theory and applications, *J. Sound Vib.*, **476**, 115316, (2020). https://doi.org/10.1016/j.jsv.2020.115316

[28] Krylov, V. V. Acoustic black holes: recent developments in the theory and applications, *IEEE T. Ultrason. Ferr.*, **61**(8), 1296–1306, (2014). https://doi.org/10.1109/TUFFC.2014.3036

[29] Zhou, X. Q. and Yu, D. Y. Acoustic energy absorption and dissipation characteristic of Helmholtz resonator enhanced and broadened by acoustic black hole, *Aerosp. Sci. Technol.*, **81**, 237–248, (2018). https://doi.org/10.1016/j.ast.2018.08.009

[30] Mironov, M. A. and Pislyakov, V. V. One-dimensional acoustic waves in retarding structures with propagation velocity tending to zero, *Acoust. Phys.*, **48**, 347–352, (2002). https://doi.org/10.1134/1.1478121

[31] Mironov, M. and Pislyakov, V. One-dimensional sonic black holes: exact analytical solution and experiments, *J. Sound Vib.*, **473**, 115223, (2020). https://doi.org/10.1016/j.jsv.2020.115223

[32] Guasch, O., Arnela, M., and Sanchez-Martin, P. Transfer matrices to calculate linear and quadratic acoustic black holes in duct terminations, *J. Sound Vib.*, **395**, 65–79, (2017). https://doi.org/10.1016/j.jsv.2017.02.007

[33] Guasch, O., Sanchez-Martin, P., and Ghilardi, D. Application of the transfer matrix approximation for wave propagation in a metafluid representing an acoustic black hole duct termination, *Appl. Math. Model.*, **77**, 1881–1893, (2020). https://doi.org/10.1016/j.apm.2019.09.039

[34] Hollkamp, J. P. and Semperlotti, F. Application of fractional order operators to the simulation of ducts with acoustic black hole terminations, *J. Sound Vib.*, **465**, 115035, (2020). https://doi.org/10.1016/j.jsv.2019.115035

[35] Zhang, X. and Cheng, L. Broadband and low frequency sound absorption by Sonic black holes with Microperforated boundaries, *J. Sound Vib.*, **512**, 116401, (2021). https://doi.org/10.1016/j.jsv.2021.116401

[36] Li, S., Xia, J., Yu, X., Zhang, X,. and Cheng, L. A sonic black hole structure with perforated boundary for slow wave generation, *J. Sound Vib.*, **559**, 117781, (2023). https://doi.org/10.1016/j.jsv.2023.117781

[37] Liang, X., Liang, H., Chu, J., Wang, W., Li, N., Yang, Z., Zhou, G., Gao, N., Hua, C., and Zhou, Z. A modified sonic black hole structure for improving and broadening sound absorption, *Appl. Acoust.*, **210**, 109440, (2023). https://doi.org/10.1016/j.apacoust.2023.109440

[38] Mousavi, A., Berggren, M., and Wadbro, E. How the waveguide acoustic black hole works: a study of possible damping mechanisms, *J. Acoust. Soc. Am.*, **151**, 4279–4290, (2022). https://doi.org/10.1121/10.0011788

[39] Cervenka, M. and Bednarik, M. On the role of resonance and thermoviscous losses in an implementation of “acoustic black hole” for sound absorption in air, *Wave Motion*, **114**, 103039, (2022). https://doi.org/10.1016/j.wavemoti.2022.103039

[40] Umnova, O., Brooke, D., Leclaire, P., and Dupont, T. Multiple resonances in lossy acoustic black holes - theory and experiment, *J. Sound Vib.*, **543**, 117377, (2023). https://doi.org/10.1016/j.jsv.2022.117377

[41] Mi, Y., Zhai, W., Cheng, L., Xi, C., and Yu, X. Wave trapping by acoustic black hole: Simultaneous reduction of sound reflection and transmission, *Appl. Phys. Lett.*, **118**(11), 114101, (2021). https://doi.org/10.1063/5.0042514

[42] Mi, Y., Cheng, L., Zhai, W., and Yu, X. Broadband low-frequency sound attenuation in duct with embedded periodic sonic black holes, *J. Sound Vib.*, **536**, 117138, (2022). https://doi.org/10.1016/j.jsv.2022.117138

[43] Stinson, M. R. The propagation of plane sound waves in narrow and wide circular tubes, and generalization to uniform tubes of arbitrary cross-sectional shape, *J. Acoust. Soc. Am.*, **89**(2), 550–558, (1991). https://doi.org/10.1121/1.400379

[44] ISO. Acoustics–determination of sound absorption coefficient and impedance in impedances tubes - part 2: Transfer-function method, ISO 10534-2, (1998).

[45] Romero-Garcìa, V., Theocharis, G., Richoux, O., and Pagneux, V. Use of complex frequency plane to design broadband and sub-wavelength absorbers, *J. Acoust. Soc. Am.*, **139**(6), 3395–3403, (2016). https://doi.org/10.1121/1.4950708

[46] Gu, T., Wen, Z., He, L., Yu, M., Li, Y., Li, Y., and Jin, Y. A lightweight metastructure for simultaneous low-frequency broadband sound absorption and vibration isolation, *J. Acoust. Soc. Am.*, **153**(1), 96–104, (2023). https://doi.org/10.1121/10.0016824